

PAPER

## Nests and chains of Hofstadter butterflies

To cite this article: Indubala I Satija and Michael Wilkinson 2020 *J. Phys. A: Math. Theor.* **53** 085703

View the [article online](#) for updates and enhancements.



**IOP | ebooks**<sup>TM</sup>

Bringing you innovative digital publishing with leading voices to create your essential collection of books in STEM research.

Start exploring the [collection](#) - download the first chapter of every title for free.

# Nests and chains of Hofstadter butterflies

Indubala I Satija<sup>1</sup>  and Michael Wilkinson<sup>2,3</sup> 

<sup>1</sup> Department of Physics, George Mason University, Fairfax, VA, United States of America

<sup>2</sup> Chan Zuckerberg Biohub, 499 Illinois Street, San Francisco, CA 94158, United States of America

<sup>3</sup> School of Mathematics and Statistics, The Open University, Walton Hall, Milton Keynes, MK7 6AA, United Kingdom

E-mail: [isatija@gmu.edu](mailto:isatija@gmu.edu) and [m.wilkinson@open.ac.uk](mailto:m.wilkinson@open.ac.uk)

Received 24 August 2019, revised 6 December 2019

Accepted for publication 20 December 2019

Published 29 January 2020



CrossMark

## Abstract

The ‘Hofstadter butterfly’, a plot of the spectrum of an electron in a two-dimensional periodic potential with a uniform magnetic field, contains subsets which resemble small, distorted images of the entire plot. We show how the sizes of these sub-images are determined, and calculate scaling factors describing their self-similar nesting, revealing an un-expected simplicity in the fractal structure of the spectrum. We also characterise semi-infinite chains of sub-images, showing one end of the chain is a result of gap closure, and the other end is at an accumulation point.

Keywords: Hofstadter butterfly, Harper equation, Chern numbers

(Some figures may appear in colour only in the online journal)

## 1. Introduction

The ‘Hofstadter butterfly’ [1] is a remarkable visual representation of the spectrum of Harper’s equation [2, 3], which is a model for Bloch electrons in a magnetic field (treated as spinless, independent particles). The butterfly plot, figure 1, shows allowed energy  $E$  plotted vertically, as a function of a parameter  $\phi$  which specifies the number of flux quanta per unit cell. The energies are plotted for values  $\phi$  which are rational numbers  $p/q$ . The allowed energies consist of  $q$  bands (with the central pair touching when  $q$  is even). As remarked by Hofstadter [1], the plot contains numerous smaller, distorted images of the whole pattern within it, largely confirming a prescient analysis of the problem made by Azbel’ [4]. Three of these distorted sub-images are highlighted in figure 1. The edges of these sub-images occur at rational values of  $\phi$ , denoted by  $\phi_R$  and  $\phi_L$  (respectively, right and left edges), and as described below, the locations of these edges follow simple number theoretical rules which are related [5] to the construction of the Farey tree [6].

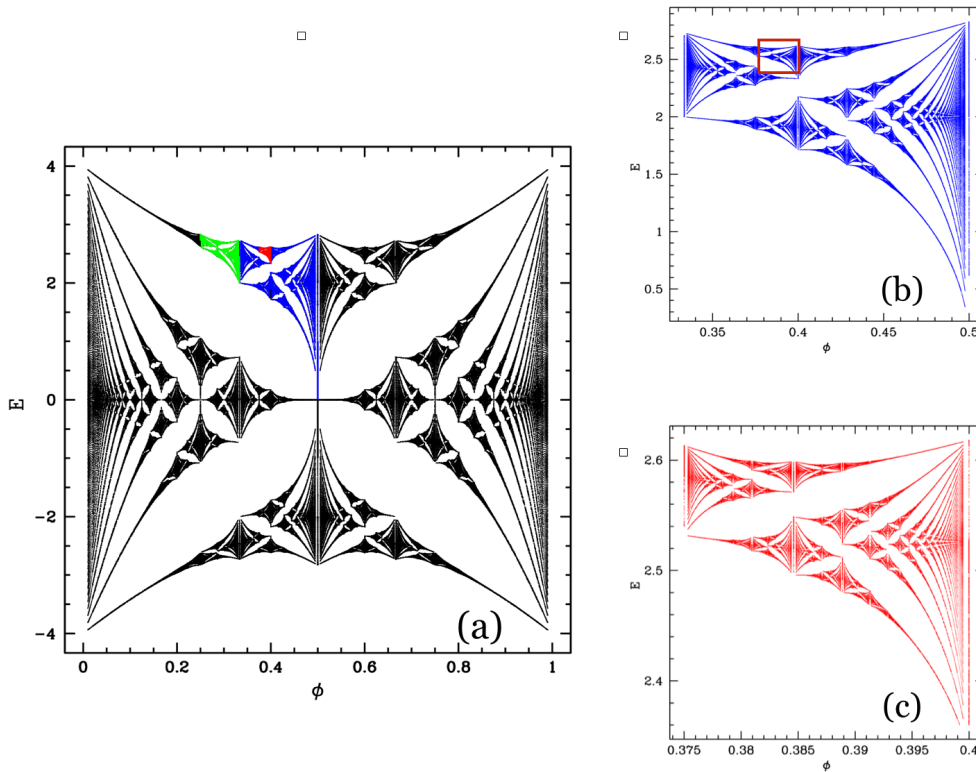


**Figure 1.** Illustrating Hofstadter’s butterfly, and three sub-images. Because the red sub-image is nested inside the blue one, in that the red sub-image has the same relationship to the blue one as the blue sub-image has to the whole plot, this nesting relationship can be made recursive, producing an infinite sequence of nested sub-images. The green and blue sub-images form adjacent links in a chain. Panel (b) and (c) show the blowups of the blue and the red part of (a). After repeated application of this nesting, the approximate similarity between the red and the blue approaches an exactly self-similar structure.

Figure 1 also illustrates two ways in which the sub-images may be related to each other. One may be nested inside the other, such as the red sub-image nesting inside the blue one. These nesting relationships can be repeated recursively, and used to characterise the extent to which the pattern is self-similar. Another possibility is for sub-images to share a common vertical edge, such as the green sub-image sharing an edge with the blue one. The sub-images can be joined in this way to create chains. The successive sub-images in a chain become smaller as we follow the chain in one direction, and we shall see that the chains are semi-infinite, ending at an accumulation point. We find that the other end of the chain is a result of gaps in the spectrum closing.

This paper will describe the rules for determining which sub-sets of the butterfly pattern can be classed as sub-images. We will show how these lead to a variety of results about constructing nests and chains of sub-images, including the calculation of scaling factors quantifying the self-similarity of Hofstadter’s plot.

The tool for this investigation will be a renormalisation-group analysis of the spectrum, originally described in [7] (a more elegant formulation was subsequently made possible using generalised Wannier functions [8, 9]). Section 2 describes the principle result on

renormalisation of  $\phi$  from [7] which is key to obtaining our results, together with new formulae for renormalisation of the quantised Hall conductance integers.

Section 3 will discuss how to label a sub-image by specifying one of its edges, and how to determine the flux value  $\phi$  for its other edge and for its centre. Recently, based upon numerical investigations, it has been proposed that these sub-images may be generated from a partition of the plot which is closely related to the Farey tree construction, and to other number-theoretical constructions, including Ford circles, integral Apollonian packings [5, 10] and Pythagorean triplets [11]. The results in section 3 explain the connection of the sub-images to the Farey tree.

Section 4 will consider how sub-images can be nested in a self-similar way, leading to exact expressions for scaling factors describing self-similar nesting. Some of these results were previously obtained by empirical observations, guided by observations of connections to the Farey tree [5, 10]. Section 5 discusses the construction of chains of sub-images. We show that they are infinite in one direction, ending in an accumulation point at a rational value of  $\phi$ , and discuss how the chains terminate at the other end due to closure of gaps in the spectrum. Our conclusions are confirmed by numerical illustrations throughout. Finally section 6 presents a summary our findings.

The Hofstadter butterfly plot has stimulated investigations which use a vast range of different methods, for example [12, 13] and [14] are significant contributions which use very different approaches from our work. There is an extensive survey of the literature in [5]. However, we are aware of one other study which emphasises making a partition of the Hofstadter butterfly plot: Osadchy and Avron [15] treat the Hofstadter plot as a phase-diagram, where the phases are labelled by quantum Hall conductances. Their approach is complementary to our own, in that their partition is based upon labelling gaps in the spectrum, rather than partitioning the spectrum itself.

## 2. Results of renormalisation group analysis

Although many aspects of the Hofstadter butterfly plot [1] are singularly discontinuous, the gaps in the spectrum of the Harper equation Hamiltonian  $\hat{H}(\phi)$  are stable features, which are continuous under variation of the flux parameter  $\phi$ . The renormalisation-group method exploits this observation, by relating the complex spectrum at a typical value of  $\phi$  to the much simpler spectrum at a nearby rational value,  $\phi = p_0/q_0$ .

Inspection of the plot shows that, when  $\phi$  is close to the rational value  $\phi_0 = p_0/q_0$ , the spectrum clusters into  $q_0$  regions, which correspond with the the  $q_0$  bands of the spectrum when  $\phi = p_0/q_0$ . In [7], it is shown that for small values of  $\phi - \phi_0$ , each of the  $q_0$  bands is transformed into the spectrum of a renormalised effective Hamiltonian operator  $\hat{H}'(\phi')$ , which has a structure which is analogous to the original problem, with a renormalised value of  $\phi$ , denoted by  $\phi'$ . The transformation is a renormalisation group because it eliminates degrees of freedom: the transformed effective Hamiltonian only describes the spectrum of one of  $q_0$  bands in the spectrum of the original Hamiltonian. In this paper we shall usually be concerned with cases where  $\phi$  is also a rational, equal to  $p/q$ . In this case the renormalised Hamiltonian also has a rational value of the flux parameter:  $\phi' = p'/q'$ , where  $p'$  and  $q'$  are integers. The relationship between between the original Hamiltonian  $\hat{H}(\phi)$  and the renormalised Hamiltonian  $\hat{H}'(\phi')$  is summarised in figure 2.

The Harper equation can be viewed as a model for either the perturbation of a Landau level by a periodic potential [16, 17], or as a model for a Bloch band perturbed by a magnetic field [2, 18]. In the former case  $\phi$  is the ratio of the area of the flux quantum to the area  $A$  of the unit cell, that is  $\phi = h/eBA$ , and in the latter case  $\phi$  is the reciprocal of this quantity. We shall

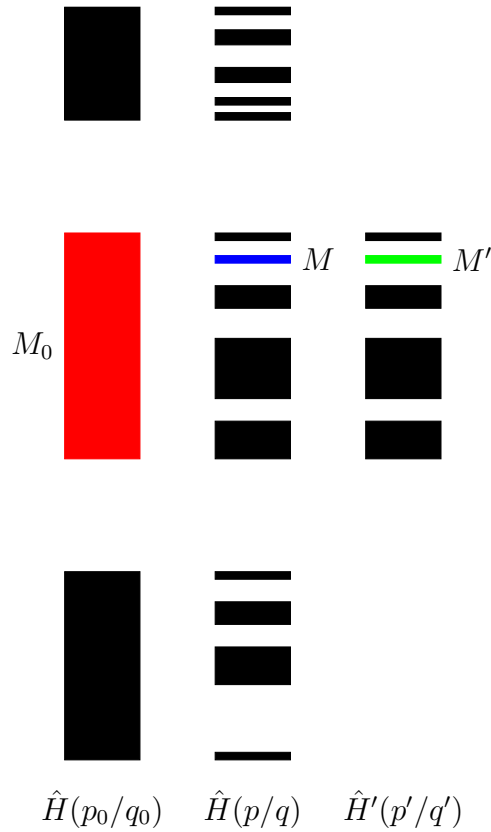


**Figure 2.** When  $\phi$  is close to  $\phi_0 = p_0/q_0$ , the spectrum of the Hamiltonian  $\hat{H}(\phi)$  divides into  $q_0$  bands. The renormalisation-group method constructs an effective Hamiltonian  $\hat{H}'$ , such that  $\hat{H}'(\phi')$  has a spectrum which is equal to the subset of the spectrum of  $\hat{H}$  contained in one of these bands. In this case we construct  $\hat{H}'(\phi')$  for a band (highlighted in red) having Hall conductance integer  $M_0$ . We are interested in the case where  $\phi = p/q$  (and consequently  $\phi' = p'/q'$ ) are rational numbers, so the spectra are sets of bands. The band highlighted in blue has Hall conductance integer  $M$ , and it corresponds to a band of  $\hat{H}'(\phi')$  (highlighted in green) with Hall conductance  $M'$ .

adopt the perturbed Landau level picture for the discussion in this paper. The total density of states in the Landau level is  $eB/h$ . When  $\phi$  is rational, the  $q$  different bands of the spectrum each has a quantised Hall conductance

$$\sigma^{(k)} = \frac{e^2}{h} M^{(k)} \tag{1}$$

where  $M^{(k)}$  is the quantised Hall conductance integer of the band with index  $k$  [19, 20]. The total Hall conductance of a single Landau level is  $\sigma^{(LL)} = e^2/h$ , so that

$$\sum_{k=1}^q M^{(k)} = 1. \tag{2}$$

### 2.1. Renormalisation of $\phi$

In [7] it is shown that the renormalised effective Hamiltonian  $\hat{H}'$  has a renormalised value of the flux parameter  $\phi$  which is given by

$$\phi' = \frac{q_0\phi - p_0}{N_0\phi + M_0} \quad (3)$$

where  $M_0$  is the quantised Hall conductance integer of the band and  $N_0$  is another integer, satisfying

$$1 = q_0M_0 + p_0N_0. \quad (4)$$

The structure of the renormalised Hamiltonian is specified by a set of Fourier coefficients,  $H'_{nm}$  [7, 21]. The evaluation of these coefficients is complicated, but analytical approximations are available when  $\phi$  is small [22, 23], and when  $\phi'$  is small [21]. For the purposes of this paper, however, we only use the fact that the renormalised Hamiltonian has a spectrum which closely resembles that of the original Hamiltonian, for a different value of  $\phi$ , and with the energies subjected to a linear transformation, as discussed in [21–23].

### 2.2. Renormalisation of $M$

Because the expression for renormalisation of  $\phi$  (equation (3)) depends upon the values of the Hall conductance integers  $M_0$  and  $N_0$ , if we are to iterate the transformation our analysis requires information about how these integers change as the renormalisation scheme is iterated. In general the Hall conductance integers  $M$  can be determined by numerically computing the Chern index of the band, as described by Thouless *et al* [19] (see also [20]), but this is cumbersome and un-informative. Instead, the recursive structure of the spectrum can be associated with a recursive method to compute the Hall conductance  $M$  of a given band. The argument was not presented in the earlier works [7–9] describing the renormalisation scheme.

Specifically, we wish to determine the Hall conductance integer  $M$  of a given band when  $\phi = p/q$ , such as the one highlighted in blue in figure 2. We shall assume that this band lies within a cluster of bands corresponding to a band of the spectrum when  $\phi = p_0/q_0$ , having Hall conductance integer  $M_0$ . This cluster of bands is described by an effective Hamiltonian  $\hat{H}'$  with  $q'$  bands, and the band highlighted in green corresponds to a band of this Hamiltonian, with Hall integer  $M'$ . In order to probe the structure of the spectrum by recursive application of the renormalisation group transformation, it would be useful to be able to express the integer  $M$  in terms of  $M_0$ ,  $M'$  and possibly other integers.

This can be achieved using the Strěda formula [24], according to which the Hall conductance when the Fermi level is in a gap is

$$\sigma = e \frac{\partial \mathcal{N}}{\partial B} \quad (5)$$

where  $\mathcal{N}$  is the number of filled states per unit area below the gap. We chose to interpret the Harper equation as representing the perturbation of a Landau level by a periodic potential, which has electron density  $eB/h$ . Then the quantity  $\phi$  is the ratio of the area of a flux quantum to the area  $A$  of the unit cell:  $\phi = h/eBA$ . If the filling fraction of the states below the band gap is  $\nu$ , we then find that

$$\sigma = \frac{e^2}{h} \left[ \nu - \phi \frac{\partial \nu}{\partial \phi} \right]. \quad (6)$$

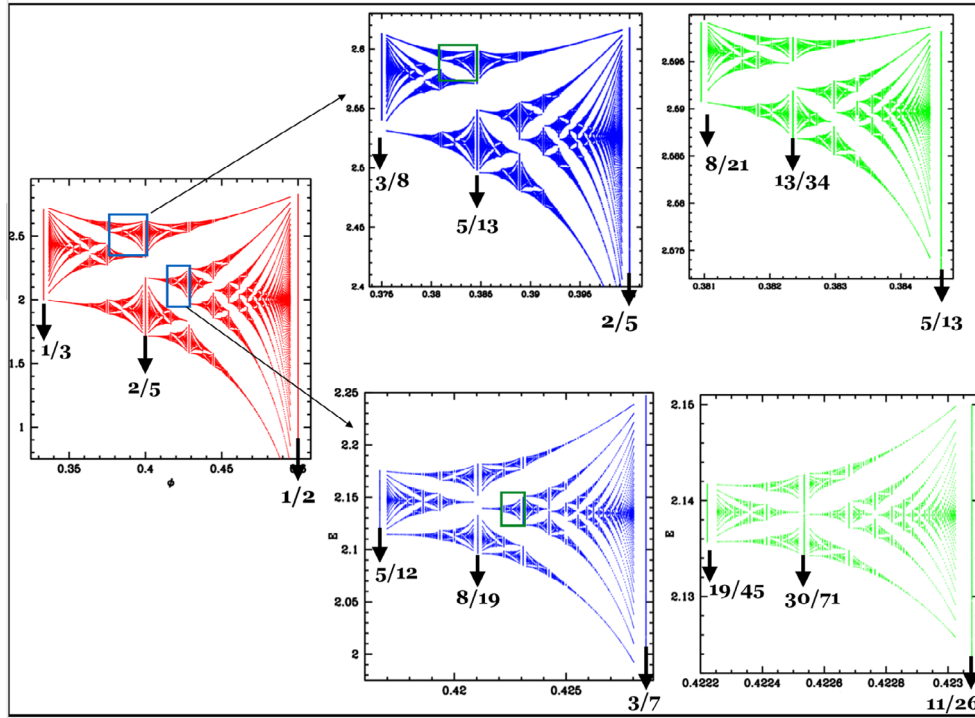


**Figure 3.** Illustrating three generations of two distinct nested sequences of sub-images that appear in the blue sub-image from figure 1. The values of  $\phi_j = p_j/q_j$  at the left-hand edge are predicted using equations (22) and (23); the values of the coefficients for this example are discussed in section 4.4. The values of  $\phi$  at the right-hand edge and at the centre of each sub-image are then obtained using equations (16) and (18), respectively.

The ‘gap-labelling theorem’ (Claro and Wannier [25]) implies that

$$\nu = \bar{N}\phi + \bar{M} \tag{7}$$

for some integers  $\bar{N}$  and  $\bar{M}$ . Substitution of (7) into (6) shows that  $\sigma = \bar{M}e^2/h$ , so that  $\bar{M}$  is the Hall conductance integer. If the spectrum is separated into several bands, we can write the filling fraction for each band in the same form as (7):

$$\Delta\nu = N\phi + M \tag{8}$$

where  $M$  is the quantised Hall conductance integer associated with a band, and  $N$  is a complementary integer.

We assume that it is possible to determine the Hall conductance integers when the denominator  $q$  of the flux ratio  $\phi = p/q$  is small. Let us approximate  $\phi$  by  $\phi_0 = p_0/q_0$ , where  $q_0$  is sufficiently small that we can readily determine the Hall integers  $M_0$ , for all of its bands, together with the conjugate integers  $N_0$  satisfying  $p_0N_0 + q_0M_0 = 1$ . We implement the renormalisation procedure of [7] using the rational  $p_0/q_0$  as the base case. We shall determine the Hall conductance integer from the spectrum alone by using the Strěda formula in the form (6).

The band for which we wish to determine the Hall conductance integer is in a cluster of bands for the  $\phi_0$  commensurability. The filling fraction of this cluster is denoted by  $\Delta\nu_0$ . The band that we are interested in lies within this cluster, and its filling fraction relative to all of the states of the cluster is  $\Delta\nu'$ . The overall filling fraction of the sub-band, which will be used to determine the Hall conductance integer, is

$$\Delta\nu(\phi) = \Delta\nu_0 \Delta\nu' . \quad (9)$$

The filling fractions are obtained by applying (8) to the original problem and to the renormalised problem in turn. The renormalised Hamiltonian has commensurability  $\phi' = p'/q'$ , and the band that we wish to analyse corresponds to a sub-band of the renormalised Hamiltonian, with gap-labelling integers  $N'$  and  $M'$ . The filling factors in (9) are, therefore,

$$\begin{aligned} \Delta\nu_0 &= N_0\phi + M_0 \\ \Delta\nu' &= N'\phi' + M' . \end{aligned} \quad (10)$$

The renormalised commensurability is given by equation (3). Substituting (10) into (9) and using (3) yields

$$\Delta\nu = (q_0N' + N_0M')\phi + (M_0M' - p_0N') . \quad (11)$$

Comparison with (8) shows that the equations for renormalisation of the Hall conductance integers are

$$M = M_0M' - p_0N', \quad N = N_0M' + q_0N' . \quad (12)$$

Note that these equations describe the quantised Hall conductance of a single band. This is sufficient for the analysis of the fine-structure of the spectrum which is pursued in this paper. For applications in which it is proposed to measure the Hall conductance, however, the Chern numbers of all of the occupied bands would have to be summed.

### 3. Labelling and construction of sub-images: relation to Farey trees

Note that, when  $\phi = 0$  or when  $\phi = 1$ , the spectrum of the Harper equation is a single interval (which happens to be  $[-4, 4]$ ). This indicates that we can define ‘sub-images’ by identifying one edge with a single band of the spectrum, bounded by a gap on either side. For example, we may take one particular band of the spectrum when  $\phi_0 = p_0/q_0$  as forming the left-hand edge of the sub-image. As we increase  $\phi$  away from its initial value of  $\phi_L = p_L/q_R$ , the spectrum becomes very complex, but the gaps which separate the sub-image from the rest of the spectrum persist. We may find that when  $\phi$  reaches another rational value,  $\phi_R = p_R/q_R$ , the complex spectrum re-forms into a single band, with the same open gaps above and below. Furthermore, the structure of the sub-spectrum in the region between  $\phi_L$  and  $\phi_R$  is well-approximated by a distorted version of the original Hofstadter butterfly.

In order to describe the sub-images we first need a convention for labelling them. We label the sub-image by specifying an energy band that forms either the left-hand or the right-hand edge. Thus a sub-image is specified using a rational number, either  $\phi_L = p_L/q_L$  or  $\phi_R = p_R/q_R$ , depending on whether we construct the sub-image by starting from its left or right edge, respectively. We must also specify the index of the band (labelling them consecutively in increasing energy). The band index will be denoted by  $k$ . According to this convention, the sub-images highlighted in figure 1, and the values of their Hall conductance integers  $N, M$ , are:

$$\begin{aligned} \text{blue} : \phi_L &= 1/3, \quad k = 3, \quad M = 0, \quad N = 1 \\ \text{red} : \phi_L &= 3/8, \quad k = 8, \quad M = -1, \quad N = 3 \\ \text{green} : \phi_L &= 1/4, \quad k = 4, \quad M = 0, \quad N = 1 . \end{aligned} \quad (13)$$



In these cases the corresponding values of the opposite edges of the sub-images are, respectively,

$$\phi_R = 1/2, \quad \phi_R = 2/5, \quad \phi_R = 1/3. \quad (14)$$

Given the value of  $\phi_L$ , we determine  $\phi_R$  by the requirement that the *renormalised* value of  $\phi$  is equal to unity at the opposite edge. Inverting (3) we obtain

$$\phi = \frac{p_0 + M_0\phi'}{q_0 - N_0\phi'}. \quad (15)$$

If we start at  $\phi_L$  (the left-hand edge), the other edge of the sub-image is obtained by setting  $\phi' = 1$ , so that on setting  $\phi_0 = \phi_L$ , equation (15) implies that  $\phi_R$  is given by

$$\phi_R \equiv \frac{p_R}{q_R} = \frac{p_L + M_0}{q_L - N_0}. \quad (16)$$

The centre of the sub-image between  $\phi_L$  and  $\phi_R$  is at a rational value  $\phi_c = p_c/q_c$ . The centre of the sub-image is defined by setting  $\phi' = \frac{1}{2}$ , so that  $\phi_c$  is given by

$$\phi_c \equiv \frac{p_c}{q_c} = \frac{M_0 + 2p_L}{2q_L - N_0}. \quad (17)$$

Thus equations (16) and (17) show that  $\phi_c$  is not the arithmetic mean of  $\phi_L$  and  $\phi_R$ , but rather

$$\frac{p_c}{q_c} = \frac{p_L + p_R}{q_L + q_R}. \quad (18)$$

This is the ‘Farey sum’ of the two edge values. Furthermore the equations (16) and (18) imply that

$$|q_L p_R - q_R p_L| = 1, \quad |q_L p_c - q_c p_L| = 1, \quad |q_R p_c - q_c p_R| = 1. \quad (19)$$

This means that the triplets  $[\frac{p_L}{q_L}, \frac{p_c}{q_c}, \frac{p_R}{q_R}]$  which are the flux values at the edges and at the centres of the sub-images are ‘neighbours’ in the Farey tree. Such triplets of rational numbers are also known as *friendly numbers*. Empirical evidence supporting (18) and (19) was previously discussed in [5, 10]. Figure 3 illustrates the application of equations (16) and (18).

## 4. Nesting of sub-images

### 4.1. Recursive nesting

The sub-images in the Hofstadter butterfly plot can be nested recursively. Here we consider how to describe and quantify this. The nested sub-images converge to a fixed point, and we can determine exact expressions for the scaling factors describing the ratio of size of different levels for the hierarchy. The fact that exact expressions for the scaling ratios can be determined is a little surprising. The crucial ingredient is that the scaling factors do not depend upon the structure of the Hamiltonian, only upon the explicit expressions for renormalisation of  $\phi$  and of the Hall integers,  $M$  and  $N$ .

We consider the following recursion. Pick a left band edge specifying a sub-image. This is described by integers  $p_0^L, q_0^L, M_0$  and  $N_0$ . We then consider a next-generation sub-image, which is obtained by picking a sub-image with the ‘internal’ coordinate of the left band edge at  $\phi' = \tilde{p}^L/\tilde{q}^L$ , with Hall conductance integers of the renormalised Hamiltonian equal to  $\tilde{M}$  and  $\tilde{N}$ . For example, in figure 1, the blue sub-image corresponds to  $p_0^L = 1, q_0^L = 3, M_0 = 0,$

$N_0 = 1$ , and the red sub-image nested inside corresponds to the same values (that is  $\tilde{p}^L = 1$ ,  $\tilde{q}^L = 3$ ,  $\tilde{M} = 0$ ,  $\tilde{N} = 1$ ).

We can then repeat this construction recursively, so that at stage  $j$ , the left band edge is  $\phi_j^L = p_j^L/q_j^L$ , and the Hall integers are  $M_j$  and  $N_j$ . At the next stage of the iteration, we determine a new band edge with its left hand edge at a *fixed* value of the *renormalised* flux parameter,  $\phi'$ , equal to  $\tilde{p}^L/\tilde{q}^L$ . The iteration of the  $\phi_j^L$  is therefore given by applying (15), replacing the  $\phi_0^L = p_0^L/q_0^L$  with the flux ratio of the left-hand band edge at level  $j$  of the nesting:

$$\phi_{j+1}^L = \frac{p_{j+1}^L}{q_{j+1}^L} = \frac{p_j^L \tilde{q}^L + M_j \tilde{p}^L}{q_j^L \tilde{q}^L - N_j \tilde{p}^L}. \quad (20)$$

The iteration of the Hall integers is obtained from (12): changing to the notation of the current application, replacing  $(M, N)$  with  $(M_j, N_j)$ , these read

$$M_{j+1} = M_j \tilde{M} - p_j^L \tilde{N}, \quad N_{j+1} = N_j \tilde{M} + q_j^L \tilde{N}. \quad (21)$$

These recursion equations describing the left-hand edges of the sub-images are a linear system of the form  $\mathbf{x}_{j+1}^L = \mathbf{A}^L \mathbf{x}_j^L$ :

$$\begin{pmatrix} p_{j+1}^L \\ M_{j+1} \\ q_{j+1}^L \\ N_{j+1} \end{pmatrix} = \mathbf{A}^L \begin{pmatrix} p_j^L \\ M_j \\ q_j^L \\ N_j \end{pmatrix} \quad (22)$$

where

$$\mathbf{A}^L = \begin{pmatrix} \tilde{q}^L & \tilde{p}^L & 0 & 0 \\ -\tilde{N} & \tilde{M} & 0 & 0 \\ 0 & 0 & \tilde{q}^L & -\tilde{p}^L \\ 0 & 0 & \tilde{N} & \tilde{M} \end{pmatrix}. \quad (23)$$

This representation is convenient because the left hand edges of the nested bands are represented by a vector  $\mathbf{x}_j^L = (p_j^L, M_j, q_j^L, N_j)$ . We observe that equations (22) and (23) can be expressed in a more elegant and symmetrical form using  $2 \times 2$  matrices:

$$\mathbf{B}_j^L = \begin{pmatrix} q_j^L & p_j^L \\ -N_j & M_j \end{pmatrix}, \quad \mathbf{C}^L = \begin{pmatrix} \tilde{q}^L & \tilde{p}^L \\ -\tilde{N} & \tilde{M} \end{pmatrix}. \quad (24)$$

Note that, as a consequence of (4), these matrices are unimodular:  $\det(\mathbf{B}_j^L) = \det(\mathbf{C}^L) = 1$ . With these definitions, equations (22) and (23) are equivalent to a matrix multiplication process:

$$\mathbf{B}_{j+1}^L = \mathbf{C}^L \mathbf{B}_j^L. \quad (25)$$

Because any unimodular  $2 \times 2$  matrix  $\mathbf{C}$  satisfies  $\mathbf{C}^2 + \mathbf{I} = \text{tr}(\mathbf{C})\mathbf{C}$  (where  $\mathbf{I}$  is the identity matrix), equation (25) can be rewritten as a set of four two-term recursions in which the variables  $(p_j, M_j, q_j, N_j)$  are decoupled:

$$s_{j+2} = (\tilde{q}^L + \tilde{M})s_{j+1} - s_j \quad (26)$$

where  $s_j$  stands for  $p_j, M_j, q_j, N_j$ .

#### 4.2. Nesting relations for right-hand edges

Instead of setting up a recursion for the left-hand edges of the nested sub-images, we could also set up a recursion for their right-hand edges. If the right hand edge of the internally nested sub-image is at a renormalised flux value of  $\tilde{\phi}^R$ , then equation (16) gives

$$\tilde{\phi}^R \equiv \frac{\tilde{p}^R}{\tilde{q}^R} = \frac{\tilde{p}^L + \tilde{M}}{\tilde{q}^L - \tilde{N}}. \quad (27)$$

The equations describing the nesting need to be modified, because the internal or renormalised coordinate of a sub-image is understood to be  $\phi' = 0$  on the left-hand edge and  $\phi' = 1$  on the right-hand edge. Equation (20) is replaced by

$$\phi_{j+1}^R = \frac{p_{j+1}^R}{q_{j+1}^R} = \frac{p_j^L \tilde{q}^R + M_j \tilde{p}^R}{q_j^L \tilde{q}^R - N_j \tilde{p}^R} = \frac{(p_j^R - M_j) \tilde{q}^R + M_j \tilde{p}^R}{(q_j^R + N_j) \tilde{q}^R - N_j \tilde{p}^R} \quad (28)$$

where the final step uses (16). Equation (21) also needs to be modified. For a sub-image based upon a band with left- and right-hand edges  $p_0^L/q_0^R$ ,  $p_0^R/q_0^R$  and with Hall conductance integers  $M_0, N_0$ , we have

$$\phi' = \frac{q_0^L \phi - p_0^L}{N_0 \phi + M_0} = \frac{(q_0^R + N_0) \phi - (p_0^R - M_0)}{N_0 \phi + M_0}. \quad (29)$$

If we replace (3) with this expression, the argument in section 2.2 leading to equation (12) now gives

$$M_{j+1} = \tilde{M}M_j - \tilde{N}(p_j^R - M_j), \quad N_{j+1} = \tilde{M}N_j + \tilde{N}(q_j^R + N_j). \quad (30)$$

The right-hand edges are described by an iteration in the form  $\mathbf{x}_{j+1}^R = \mathbf{A}^R \mathbf{x}_j^R$  where  $\mathbf{x}_j^R = (p_j^R, M_j, q_j^R, N_j)$  and

$$\mathbf{A}^R = \begin{pmatrix} \tilde{q}^R & \tilde{p}^R - \tilde{q}^R & 0 & 0 \\ -\tilde{N} & \tilde{M} + \tilde{N} & 0 & 0 \\ 0 & 0 & \tilde{q}^R & -(\tilde{p}^R - \tilde{q}^R) \\ 0 & 0 & \tilde{N} & \tilde{M} + \tilde{N} \end{pmatrix}. \quad (31)$$

Alternatively, we can write the iteration in the form of equations (24) and (25), with  $\mathbf{C}^L$  replaced by

$$\mathbf{C}^R = \begin{pmatrix} \tilde{q}^R & \tilde{p}^R - \tilde{q}^R \\ -\tilde{N} & \tilde{M} + \tilde{N} \end{pmatrix}. \quad (32)$$

#### 4.3. Scaling factors

The eigenvalues of the matrix (23) are two doubly-degenerate pairs. Noting equation (4) (in the form  $1 = \tilde{q}\tilde{M} + \tilde{p}\tilde{N}$ ), they are equal to

$$\lambda_{\pm} = \frac{(\tilde{q}^L + \tilde{M})}{2} \pm \sqrt{\left(\frac{\tilde{q}^L + \tilde{M}}{2}\right)^2 - 1}. \quad (33)$$

The values of  $\tilde{p}^L$ ,  $\tilde{q}^L$  and  $\tilde{M}$  describe how the nested sequences of sub-images are constructed. We consider a band with left edge  $\phi_0^L = p_0^L/q_0^L$ , with Hall conductance  $M_0$ , and its corresponding sub-image. We can recursively construct sub-images nested within this one, with

an ‘internal’ or renormalised flux at the left edge equal to  $\phi' = \tilde{p}^L/\tilde{q}^L$ . The Hall conductance integers of the renormalised Hamiltonian are  $\tilde{M}, \tilde{N}$ . In terms of the full-scale Hofstadter butterfly plot, the left edge of the new sub-image is  $\phi_1^L = p_1^L/q_1^L$ . We can then recursively construct further sub-images in the same manner, with their left edges at flux values  $\phi_j^L = p_j^L/q_j^L$ . The  $\phi_j^L$  may be obtained by iteration of (22) with initial values  $\mathbf{x}_0^L = (p_0^L, M_0, q_0^L, N_0)$ , and the corresponding right-hand edges are obtained using (16). The bands constructed by iteration of this procedure converge towards a point in the original Hofstadter butterfly plot as the transformation is iterated. The sizes of the sub-images decrease with each iteration: their horizontal extent is

$$\Delta\phi_j = |\phi_j^L - \phi_j^R| = \left| \frac{p_j^L q_j^R - q_j^L p_j^R}{q_j^L q_j^R} \right|. \tag{34}$$

Using (19), we obtain

$$\Delta\phi_j = \frac{1}{q_j^L q_j^R}. \tag{35}$$

As  $j \rightarrow \infty$  the solutions of (22) are determined by the eigenvalues of  $\mathbf{A}^L$  which have the largest magnitude. These will be denoted by  $\lambda_*$ . Note that, because  $\tilde{q}^R = \tilde{q}^L - \tilde{N}$ , the matrices  $\mathbf{A}^L$  and  $\mathbf{A}^R$  have the same eigenvalues. The scaling ratio between the sizes of successive sub-images therefore approaches a limit

$$\lim_{j \rightarrow \infty} \frac{\Delta\phi_{j+1}}{\Delta\phi_j} = \frac{1}{\lambda_*^2} \tag{36}$$

where  $\lambda_*$  is the larger in magnitude of the  $\lambda_{\pm}$  obtained from equation (33). The values of  $M_j$  and  $N_j$  also grow under iteration of the map (22): in this case the ratio of successive values is asymptotic to the eigenvalue with the largest magnitude,  $\lambda_*$ : we have

$$\lim_{j \rightarrow \infty} \frac{M_{j+1}}{M_j} = \lim_{j \rightarrow \infty} \frac{N_{j+1}}{N_j} = \lim_{j \rightarrow \infty} \frac{p_{j+1}^X}{p_j^X} = \lim_{j \rightarrow \infty} \frac{q_{j+1}^X}{q_j^X} = \lambda_* \tag{37}$$

where, X may stand for L, c or R, so that  $\phi_j^X = p_j^X/q_j^X$  is the flux parameter at, respectively, the left hand edge, the centre, or the right-hand edge of the sub-image after  $j$  iterations. Therefore, as we zoom in the (asymptotically) self-similar sequence of sub-images, their flux intervals shrink by the scaling factor  $\lambda_*^2$ . The topological integers  $(M_j, N_j)$  and the numerator  $p_j^X$  and the denominator  $q_j^X$  of the rational flux  $\phi_j^X = \frac{p_j^X}{q_j^X}$  (with X = L, R, c) grow by the scaling factor  $\lambda_*$ . We will refer to  $\lambda_*$  as the *scaling factor* for the set of nested sub-images. Equations (36) and (37) show that  $\lambda_*$ , which is a simple function of the integer  $\tilde{q}^L + \tilde{M}$ , characterises many aspects of the self-similarities which are contained in the butterfly plot.

#### 4.4. Examples

Figure 3 shows two examples of nested sequences of sub-images. We consider an initial sub-image, the one shown in blue in figure 1, with  $\phi_L = 1/3, k = 3$ , (for which  $M = 0, N = 1$ , and hence  $\phi_R = 1/2$ ), and then build two sequences of nested sub-images of this.

In the upper panels of figure 3 we follow a nested sequence of sub-images of the red sub-image of figure 1, with  $\phi_L = 1/3, k = 3$  (for which  $M = 0, N = 1$ , implying  $\phi_R = 1/2$ ), which

has the same relation to the first sub-image as that sub-image has to the entire Hofstadter plot. We iterate equations (22) and (23) with the initial conditions

$$\mathbf{x}_0^L = (p_0^L, M_0, q_0^L, N_0) = (1, 0, 3, 1). \quad (38)$$

We then use the following values in equation (23) to determine the matrix  $\mathbf{A}^L$ :

$$(\tilde{p}^L, \tilde{M}, \tilde{q}^L, \tilde{N}) = (1, 0, 3, 1). \quad (39)$$

Iteration of equation (23) then gives the following for the first three iterates:

$$\begin{aligned} \mathbf{x}_1^L &= (p_1^L, M_1, q_1^L, N_1) = (3, -1, 8, 3) \\ \mathbf{x}_2^L &= (p_2^L, M_2, q_2^L, N_2) = (8, -3, 21, 8) \\ \mathbf{x}_3^L &= (p_3^L, M_3, q_3^L, N_3) = (21, -8, 55, 21). \end{aligned} \quad (40)$$

The corresponding right-hand edges and centre points are then obtained using the values of  $M_j$  and  $N_j$  in equation (44), together with equations (16) and (18). We find the following values for the three generations:

$$\begin{aligned} \text{First generation: } \phi_L &= 3/8, \phi_R = 2/5, \phi_c = 5/13 \\ \text{Second generation: } \phi_L &= 8/21, \phi_R = 5/13, \phi_c = 13/34 \\ \text{Third generation: } \phi_L &= 21/55, \phi_R = 13/34, \phi_c = 55/89. \end{aligned} \quad (41)$$

In this example, eigenvalues are  $\lambda_{\pm} = (3 \pm \sqrt{5})/2$ , so that the ratio of the sizes of the nested sub-images approaches  $((3 + \sqrt{5})/2)^2 = (7 + 3\sqrt{5})/2$ .

In the lower sequence of figure 3 we follow a nested sequence of sub-images of the blue sub-image from figure 1, this time based upon a nested sequence of sub-images for which the ‘internal’ or renormalised coordinate of the left-hand edge is  $\tilde{\phi} = 3/5$ , with band index  $k = 3$ . For this band the Hall conductance integers are  $\tilde{M} = -1$ ,  $\tilde{N} = 2$ , implying that the right-hand edge has internal coordinate  $\tilde{\phi}_R = 2/3$ . Accordingly, we iterate equations (22) and (23) with the same initial conditions

$$\mathbf{x}_0^L = (p_0^L, M_0, q_0^L, N_0) = (1, 0, 3, 1) \quad (42)$$

and we use the following values in equation (23) to determine the matrix  $\mathbf{A}^L$ :

$$(\tilde{p}^L, \tilde{M}, \tilde{q}^L, \tilde{N}) = (3, -1, 5, 2). \quad (43)$$

Iteration of equation (23) then gives the following for the first three iterates:

$$\begin{aligned} \mathbf{x}_1^L &= (p_1^L, M_1, q_1^L, N_1) = (5, -2, 12, 5) \\ \mathbf{x}_2^L &= (p_2^L, M_2, q_2^L, N_2) = (19, -8, 45, 19) \\ \mathbf{x}_3^L &= (p_3^L, M_3, q_3^L, N_3) = (71, -30, 168, 71). \end{aligned} \quad (44)$$

From these vectors we extract the following values for the left-hand edges  $\phi_j^L$  of a nested sequence of sub-images:  $\phi_1^L = 5/12$ ,  $\phi_2^L = 19/45$ ,  $\phi_3^L = 71/168, \dots$  We predict that there will be generations of nested sub-images with the following edges and centres

**Table 1.** Four infinite chains of sub-images (labelled by  $C_{\frac{p_{cl}}{q_{cl}} \rightarrow \frac{p_{ac}}{q_{ac}}, k \pm}$ , where  $\frac{p_{cl}}{q_{cl}}$  is the open edge, and  $\frac{p_{ac}}{q_{ac}}$  is the accumulation point, attaching to band  $k$ , at the the upper, +, or lower edge, -, edge). We list the flux parameter of one edge of a sub-image,  $p_j/q_j$ , with  $j = 0$  giving the closed edge and  $j = 1, 2, \dots$  giving the open edges, the values of the Hall integers for the chain,  $(M_0, N_0)$ , and the colour used to highlight the chain in figure 4.

$C_{\frac{p_{cl}}{q_{cl}} \rightarrow \frac{p_{ac}}{q_{ac}}, k \pm}$	$\frac{p_j}{q_j}$	$(M_0, N_0)$	Colour
$C_{\frac{1}{2} \rightarrow 0, 1+}$	$\frac{1}{j+1}$	(0, 1)	Red
$C_{0 \rightarrow \frac{1}{2}, 1+, 2-}$	$\frac{j-1}{2j-1}$	(1, -2)	Blue
$C_{\frac{1}{3} \rightarrow \frac{1}{4}, 2+, 3-}$	$\frac{1+j}{3+4j}$	(-1, 4)	Green
$C_{\frac{1}{4} \rightarrow \frac{1}{3}, 2+}$	$\frac{j+1}{3j+4}$	(1, -3)	Purple

First generation:  $\phi_L = 1/3, \phi_R = 1/2, \phi_c = 2/5$

Second generation:  $\phi_L = 5/12, \phi_R = 3/7, \phi_c = 8/21$

Third generation:  $\phi_L = 19/45, \phi_R = 11/26, \phi_c = 30/71$ . (45)

In this case the eigenvalues are  $\lambda_{\pm} = 2 \pm \sqrt{3}$ , so that the ratio of the sizes of the nested sub-images approaches  $(2 + \sqrt{3})^2 = 7 + 4\sqrt{3}$ .

#### 4.5. A simplified recursion

The recursions (22) and (23) describing the nesting of sub-images are coupled equations in  $\phi_j^L$  and the Hall conductances integers,  $M_j$  and  $N_j$ . We noticed that, in the special case where we the parameters of the initial sub-images and those of the subsequent nesting are the same (that is, when  $\{\tilde{p}^L, \tilde{q}^L, \tilde{M}, \tilde{N}\} = \{p_0^L, q_0^L, M_0, N_0\}$ ), the flux parameters  $\phi_j$  satisfy a very simple recursion, which does not require information about the Hall conductance integers  $M_j$  and  $N_j$ . In the special case where

$$\mathbf{x}_0^L = (p_0^L, M_0, q_0^L, N_0) = (\tilde{p}^L, \tilde{M}, \tilde{q}^L, \tilde{N}) \tag{46}$$

we find that the recursion of the  $\phi_j^L$  is given by

$$\phi_{j+1} = \frac{\tilde{p} + \tilde{M}\phi_j}{\tilde{q} - \tilde{N}\phi_j}. \tag{47}$$

This is simpler than (20) because it uses the *fixed* Hall conductances  $\tilde{M}$  and  $\tilde{N}$ , rather than  $M_j$  and  $N_j$ , which depend of the index of the iteration,  $j$ . The form of equation (47) bears a marked similarity to (15), but we cannot deduce it directly from that equation. Instead we must show how it arises from equations (22) and (23) in the special case where (46) is satisfied.

We can obtain  $\phi_j^L = p_j^L/q_j^L$  from the first and third coefficients of  $\mathbf{x}_j^L = (\mathbf{A}^L)^j \mathbf{x}_0^L$ . Note that, in the special case that we consider,

$$\mathbf{A}^L \mathbf{x}_0^L = (\tilde{q}^L + \tilde{M})\mathbf{x}_0^L - \mathbf{y}_0, \quad \mathbf{y}_0 = (0, 1, 1, 0), \quad \mathbf{A}^L \mathbf{y}_0 = \mathbf{x}_0 \tag{48}$$

and hence deduce that

$$\mathbf{x}_j^L \equiv (\mathbf{A}^L)^j \mathbf{x}_0^L = \alpha_j \mathbf{x}_0^L + \beta_j \mathbf{y}_0. \tag{49}$$

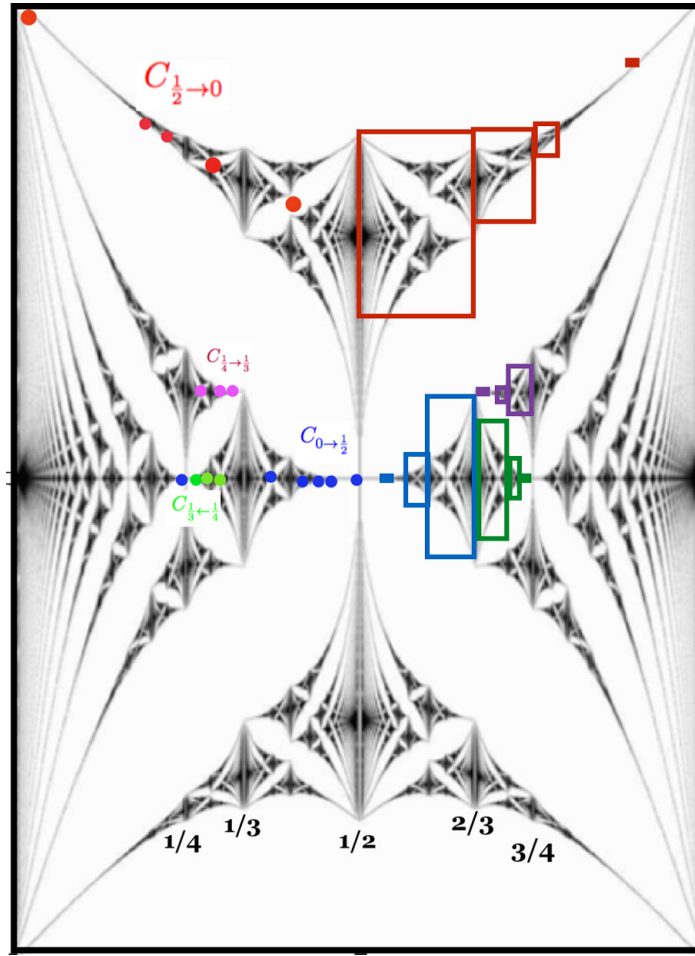


**Figure 4.** Illustrating examples of four chains (colour coded in red, blue, green and purple) of sub-images, specified in table 1. Exploiting left-right symmetry of the graph, chains are shown in two ways. On the left, each member of the chain is shown with a dot at the centre of the sub-image and on the right, the sub-images are shown in the boxes. The ends of the chains are specified by the accumulation points and the closed edges listed in table 1. For example, the purple chain lies between the third band at  $\phi = 1/4$  (which closes on its lower edge) and an accumulation point at  $\phi = 1/3$ .

Using (48) we find that the coefficients  $\alpha_j, \beta_j$  satisfy

$$\begin{pmatrix} \alpha_{j+1} \\ \beta_{j+1} \end{pmatrix} = \mathbf{a} \begin{pmatrix} \alpha_j \\ \beta_j \end{pmatrix}, \quad \mathbf{a} = \begin{pmatrix} \tilde{q} + \tilde{M} & 1 \\ -1 & 0 \end{pmatrix}. \tag{50}$$

From (48) and (49) we deduce that  $p_j = \tilde{p}\alpha_j$  and  $q_j = \tilde{q}\alpha_j + \beta_j$ , so that (50) can be expressed as a recursion of  $\{p_j^L, q_j^L\}$ , in the form

$$\begin{pmatrix} p_{j+1}^L \\ q_{j+1}^L \end{pmatrix} = \begin{pmatrix} \tilde{M} & \tilde{p} \\ -\tilde{N} & \tilde{q} \end{pmatrix} \begin{pmatrix} p_j^L \\ q_j^L \end{pmatrix}. \tag{51}$$

Equation (47) then follows immediately. It is easy to check that equation (47) reproduces the left-hand band edges in the upper panel of figure 3. It does not reproduce the values of  $\phi_j^L$  for the lower panel, because these do not satisfy (46).

In the special case where (46) applies, we can determine the accumulation point  $\phi_*$  of the nesting process as the fixed point of equation (47). Setting  $\phi_{j+1} = \phi_j = \phi_*$ , we find

$$\phi_* = \frac{1}{2N} \left[ (\tilde{q} - \tilde{M}) \pm \sqrt{(\tilde{q} + \tilde{M})^2 - 4} \right] \quad (52)$$

(with the sign chosen so that  $0 < \phi_* < 1$ ). We remark that the sequences  $\phi_j^L, \phi_j^R$  bracket this accumulation point, and that  $\phi_j^c$  is another sequence that converges towards it. In the general case none of these sequences corresponds to the continued fraction representation of  $\phi_*$ .

### 5. Chains of sub-images

The arguments of section 3 show that each of the  $q_0$  bands of the spectrum at  $\phi = p_0/q_0$  is potentially an edge of two different sub-images: setting  $\phi' = \pm 1$ , we see that the other edges of these two connected sub-images are at

$$\phi_{\pm} = \frac{p_0 \pm M_0}{q_0 \mp N_0}. \quad (53)$$

These two values can themselves be the edges of further sub-images. Because  $N_0$  and  $M_0$  are constant so long as gaps do not close, by iteration we have a sequence of edges of a connected chain of sub-butterflies, for which the values of  $\phi$  are

$$\phi_j = \frac{p_0 + jM_0}{q_0 - jN_0} \quad (54)$$

where  $j$  is a positive or negative integer.

The sub-images are constructed by taking a band at  $\phi_0 = p_0/q_0$  and increasing  $\phi$  until the renormalised value  $\phi'$  is equal to unity, at which point the spectrum of the renormalised Hamiltonian is, once again, a single band. The results in [7] do not guarantee that extrapolation to  $\phi' = 1$  is possible, and one way in which the procedure could fail is if the gaps which exist in the spectrum when  $\phi' = 0$  close up as  $|\phi'|$  increases. We find, for a given value of  $\phi_0 = p_0/q_0$ , that it is always possible to construct a sub-image of the butterfly plot to either the right (setting  $\phi' = +1$ ) or the left, ( $\phi' = -1$ ) without gaps in the spectrum closing, but not always both. We refer to sub-images which have *both* upper and lower gaps open at *both* sides as *open* sub-images. Other sub-images will be termed *closed*.

In cases where the gaps close, we find empirically that this occurs when  $|\phi'| = 1$ . As an example, consider the case of the centre band for  $\phi_0 = 1/3$  (for this band  $M = 1, N = -2$ ). Applying (53) we find  $\phi_+ = 2/5$  and  $\phi_- = 0$ . There is an open sub-image for the centre band which is bounded by  $\phi_L = 1/3$  and  $\phi_R = 2/5$ , but if we consider how the centre band for  $\phi_R = 1/3$  evolves as we approach  $\phi_L = 0$ , we see that the gaps at both the top and the bottom of the band close up as we approach  $\phi = 0$ . There are other examples where only one of the gaps closes: for example let us consider the uppermost band when  $\phi_0 = 2/5$  (which has  $M = 1, N = -2$ ). In this case  $\phi_+ = 3/7$  and  $\phi_- = 1/3$ . There is an open sub-image containing the uppermost band bounded by  $\phi_L = 2/5$  and  $\phi_R = 3/7$ , but if we extend the uppermost band from  $\phi_R = 2/5$  towards  $\phi_L = 1/3$ , we find that the lower gap closes, so that we have a closed sub-image.



In cases where the sub-image is ‘open’, the formulae for predicting the  $\phi$  value of one edge from the other can be used reciprocally: we can determine  $\phi_R$  from  $\phi_L$  by taking the positive sign in (53), or  $\phi_L$  from  $\phi_R$  by taking the negative sign. If, however, the sub-image has a closed gap at the right-hand side, while it is possible to compute  $\phi_R$  from  $\phi_L$ , if we start from  $\phi_R$ , the values of the Hall conductance integers are changed by the additional component of the spectrum which does not form part of the band at  $\phi_L$ .

It is also possible for a ‘closed’ edge to be shared between multiple sub-images. An example of this is the set of centre bands at a sequence of values  $\phi_R = 1/(2n + 1)$ , with  $n = 1, 2, \dots$ . Here  $M = 1$  and  $N = -2n$ . If we apply equation (53) with the negative sign, we find that the left hand edge is  $\phi_L = 0$  in every case. We find that the left-hand edge of each sub-image based upon the centre band at  $\phi_R = 1/(2n + 1)$  is the entire spectrum at  $\phi = 0$ , for all integer  $n > 0$ . The reason why this band can be the left hand edge of an infinite number of different sub-images is that, as  $\phi \rightarrow 0$ , an infinite number of bands accumulate at both the upper and lower edges of the spectrum.

For every band at a rational value of  $\phi$ , we can attempt to construct a connected chain of sub-images extending in either direction using equation (54). We find that the chain terminates in one direction, due to encountering an edge where the gaps close. The chain extends to infinite values of  $|j|$  in the other direction. Note that  $\phi_j$ , defined by (54), approaches  $-M_0/N_0$  as  $|j| \rightarrow \infty$ , so that the chain of sub-images ends at an accumulation point. For example, every centre band for  $\phi = 1/(2n + 1)$  (with  $n = 1, 2, \dots$ , having Hall integers  $M_0 = 1$  and  $N_0 = -2n$ ) has a chain of sub-images extending to the right, with edges  $\phi_j = (j + 1)/[2n(j + 1) + 1]$ , end at an accumulation point at  $\phi = 1/2n$ .

Table 1 lists parameters of four different examples of chains, which are illustrated in figure 4. The chains are denoted by a label  $C_{\frac{p_{cl}}{q_{cl}} \rightarrow \frac{p_{ac}}{q_{ac}}, k_{\pm}}$  in which  $p_{cl}/q_{cl}$  is the closed edge and  $p_{ac}/q_{ac}$  is the accumulation point, and  $k$  labels the band to which the accumulation point attaches, with  $\pm$  indicating whether the attachment is to the top  $+$ , or bottom  $-$ . The edges of the sub-images forming the chain are denoted by  $\phi_j$ , with  $j = 0$  being the edge for which a gap closes, and  $j = 1, 2, \dots$  being labels of the open edges.

## 6. Summary

A striking feature of Hofstadter’s butterfly is the fact that its interior can be dissected into small, distorted images of the entire plot. These sub-images are a microcosm of the butterfly plot.

In this work we have described how every band of the spectrum for rational  $\phi$  can be taken to be an edge of at least one sub-image, and we have shown how the other edge or edges can be determined. The centre and the edges are shown to be neighbouring fractions in the Farey tree and the equations relating them depend upon the quantised Hall conductance integers,  $M$  and  $N$ .

We have also analysed two ways in which these objects can be interrelated, namely by being recursively nested, or by forming chains. Each sub-image is described by four integers:  $p$  and  $q$  specify the flux ratio (on one of the edges), and  $M, N$  specify its associated quantised Hall conductance. Both the nesting and concatenation relationships between sub-images are represented by simple algebraic operations on the set  $\{p, M, q, N\}$ . Equations (24) and (25) show that nesting relationship may be represented by multiplication of  $2 \times 2$  unimodular matrices composed from these numbers. Equation (54) shows that the concatenation relation corresponds to a simple additive relation.

The nesting relationship leads to the derivation of exact expressions for the scaling factors describing self-similarity. The sub-images are described by rational fluxes at every step of the recursion, but their asymptotic scaling factors and accumulation points (equations (33) and (52) respectively) are irrational numbers, obeying simple integer-coefficient quadratic equations. It is surprising that the scaling factors do not require the solution of matrix eigenvalue equations. It can also be noted that the set of quadratic numbers which can arise from equation (33) does not include the golden mean,  $(1 + \sqrt{5})/2$ , which features so extensively in the literature on Harper's equation, reviewed in [5]. The chains are infinite in one direction, with successively smaller sub-butterflies reaching an accumulation point. In contrast to the accumulation points of the nesting process, the chains end at a rational value of  $\phi$ .

## Acknowledgments

IIS thanks the Department of Mathematics and Statistics at the Open University, where this work was started. MW thanks the Physics Department of George Mason University for its hospitality.

## ORCID iDs

Indubala I Satija  <https://orcid.org/0000-0001-8694-6283>

Michael Wilkinson  <https://orcid.org/0000-0002-5131-9295>

## References

- [1] Hofstadter D R 1976 Energy-levels and Wave-functions for Bloch electrons in rational and irrational magnetic fields *Phys. Rev. B* **14** 2239–49
- [2] Peierls R 1933 On the theory of diamagnetism of conduction electrons *Z. Phys.* **80** 763–91
- [3] Harper P G 1955 Single band motion of conduction electrons in a uniform magnetic field *Proc. Phys. Soc. A* **68** 879
- [4] Azbel M Y 1964 *Zh. Eksp. Teor. Fiz.* **46** 929  
Azbel M Y 1964 Energy spectrum of a conduction electron in a magnetic field *Sov. Phys.—JETP* **19** 634–45 (Engl. transl.)
- [5] Satija I I 2016 *Butterfly in the Quantum World: the Story of the Most Fascinating Quantum Fractal* (Bristol: Morgan & Claypool)
- [6] Hardy G H and Wright E M 1979 *An Introduction to the Theory of Numbers* 5th edn (Oxford: Oxford University Press)
- [7] Wilkinson M 1987 An exact renormalisation group for bloch electrons in a magnetic field *J. Phys. A: Math. Gen.* **20** 4337–54
- [8] Wilkinson M 1998 Wannier functions for lattices in a magnetic field *J. Phys.: Condens. Matter* **10** 7407–27
- [9] Wilkinson M 2000 Wannier functions for lattices in a magnetic field II: extension to irrational fields *J. Phys.: Condens. Matter* **12** 4993–5009
- [10] Satija I I 2016 A tale of two fractals: the Hofstadter butterfly and the integral apollonian gaskets *Eur. Phys. J.* **225** 2533–47
- [11] Satija I I 2018 Pythagorean triplets, integral apollonians and the Hofstadter butterfly (arXiv:1802.04585v3 [nlin.CD])
- [12] Wiegmann P and Zabrodin A V 1994 Quantum group and magnetic translations Bethe ansatz for the Asbel-Hofstadter problem *Nucl. Phys. B* **422** 495–514
- [13] Faddeev L D and Kashaev R M 1995 Generalized Bethe ansatz equations for Hofstadter problem *Commun. Math. Phys.* **169** 181–91

- [14] Last Y 1994 Zero measure spectrum for the almost mathieu operator *Commun. Math. Phys.* **164** 421–32
- [15] Osadchy D and Avron J E 2001 Hofstadter butterfly as quantum phase diagram *J. Math. Phys.* **42** 5665–71
- [16] Schellnhuber H J, Obermair G M and Rauh A 1981 First-principles calculation of dimagnetic band-structure II: spectrum and wave-functions *Phys. Rev. B* **23** 5191–202
- [17] Wilkinson M 1987 An exact effective Hamiltonian for a perturbed Landau level *J. Phys. A: Math. Gen.* **20** 1761–71
- [18] Roth L M 1962 Theory of bloch electrons in a magnetic field *J. Phys. Chem. Solids* **23** 433
- [19] Thouless D J, Kohmoto M, Nightingale M P and den Nijs M 1982 Quantised Hall conductance in a two-dimensional periodic potential *Phys. Rev. Lett.* **49** 405–8
- [20] Dana I, Avron Y and Zak J 1985 Quantised Hall conductance in a perfect crystal *J. Phys. C: Solid State Phys.* **18** L679–84
- [21] Wilkinson M and Kay R J 1996 Semiclassical limits of the spectrum of Harper’s equation *Phys. Rev. Lett.* **76** 1896–9
- [22] Suslov I M 1982 *Zh. Eksp. Teor. Fiz.* **83** 1079–88  
Suslov I M 1982 Localisation in one-dimensional incommensurable systems *Sov. Phys.—JETP* **56** 612–7 (Engl. transl.)
- [23] Wilkinson M 1984 Critical properties of electron eigenstates in incommensurate systems *Proc. Roy. Soc. A* 391 305–50
- [24] Strěda P 1982 Theory of quantised Hall conductivity in two dimensions *J. Phys. C: Solid State Phys.* **15** L717–21
- [25] Claro F H and Wannier G H 1979 Magnetic subband structure of electrons in hexagonal lattices *Phys. Rev. B* **19** 6068–74